

## DOPPLER INFORMATION EXTRACTION OF SEGMENT SIGNAL USING S-MVDR METHOD IN HFSWR

SHANG SHANG<sup>1,2</sup>, YANG LI<sup>2</sup>, NING ZHANG<sup>2</sup> AND ZHAO-BIN WANG<sup>3</sup>

<sup>1</sup>No. 38 Research Institute of CETC  
No. 199, Xiangzhang Road, Hefei 230038, P. R. China  
shangshang@hit.edu.cn

<sup>2</sup>School of Electronics and Information Engineering  
Harbin Institute of Technology  
No. 92, West Da-Zhi Street, Harbin 150001, P. R. China  
{li.yang; zhangn}@hit.edu.cn

<sup>3</sup>School of Electronics and Information  
Jiangsu University of Science and Technology  
No. 2, Mengxi Road, Zhenjiang 212003, P. R. China  
Wangzb\_just@163.com

Received November 2011; revised March 2012

**ABSTRACT.** *This paper proposes a novel spectrum estimation algorithm in order to extract the Doppler information of segment echo data of high frequency surface wave radar (HFSWR) operating at sweep frequency mode. Working in this mode, the HFSWR can avoid interferences related to radar frequency, such as ionospheric clutter, sea clutter, and cochannel interference. However, the echo signals operating at the same frequency are segmental due to the random phase differences among echo segments. It is difficult to extract Doppler information of the specific data since the monitoring time of each segment is short. To solve this problem, this paper establishes a model of echo signal in the sweep frequency mode, and proposes an improved S-MVDR (segment-minimum variance distortionless response) algorithm according to the characteristics of the signal model. It is demonstrated by theoretical analysis that the S-MVDR algorithm can improve the resolution of the spectrum estimation without losing any frequency information. Simulations show that the S-MVDR algorithm has higher resolution and signal noise ratio than other segment signal spectrum estimation algorithms.*

**Keywords:** HFSWR, Doppler frequency, Spectral estimation, MVDR, S-MVDR

**1. Introduction.** The HFSWR transmits signals at the horizontal angle and detects targets (such as low altitude aircrafts, ships and aerodynamic missiles [1,2]) utilizing the transmitting capacity of vertical polarization electromagnetic wave along the sea surface. In addition, it can extract sea state information of ocean current, velocity and direction of the sea surface wind field, and wave height [3-5]. The HFSWR can compensate for the blind zone of sky wave radar and microwave radar. Its detection range is 200-400km in general. Meanwhile, the HFSWR has the advantages of anti-jamming, anti-extra-low-altitude raid, anti-stealth, countermeasure against anti-radiation missile, anti-ARM and low cost. In addition, it adopts wide-beam and digital beam forming techniques [6]. Therefore, it can be considered as an ideal early warning radar, and can be used for coast monitoring, sea state remote sensing, ocean surface pollution monitoring [7], resource development, etc.

However, the HFSWR also has some limitations and weaknesses. Due to the nonideality of transmitting antenna, some wave energy radiates upward and is reflected by the

ionosphere. The energy received by the receiving antenna forms ionospheric clutter. The ionospheric clutter affects the detection performance of the HFSWR [8-10] beyond 100km [11]. Since the accurate detection is the precondition of early warning and tracking [12], many scholars have made plenty of researches on ionospheric clutter suppression, but there is no effective technique, which fits all sort of conditions because of the complexity of the formation and changes in the clutters. As a result, the ionospheric clutter has become a bottleneck in the development of HFSWR [13].

The ionospheric clutter is caused by the ionosphere reflection of electromagnetic wave, and the influence is closely related to wave frequency. In the simplest condition of normal incidence, for example, the wave with specific frequency incidences into the ionosphere and reflects back to the ground at the height where the plasma frequency is equal to the wave frequency. Each layer in ionosphere reflects different frequency which forms the ionospheric clutter. The physical parameters (i.e., plasma frequency, electron concentration and moving speed) of each layer are different and time varying, so the ionospheric clutter in the HFSWR operating on different frequency is not the same. Frequency agility is an effective method to avoid the influence from ionospheric clutter [14]. Nevertheless, the problem is that it will pollute many frequencies. Therefore, we intend to design such a HFSWR system with sweep frequency mechanism that the echo data of different frequencies can compensate each other to improve the detection performance.

Radar monitors the optional frequencies provided by the spectrum monitoring subsystem in sequence on sweep frequency mode. To ensure real-time results, the monitoring time of each frequency is short, and a second sweep frequency is taken after all frequencies are completed for the first round. After taking sweep frequency for several times, the echoes of the same frequency are properly processed. This working mode allows us to monitor the optional frequencies within the total monitoring time by the way of time period sampling, and the results can better reflect the overall situation within the total monitoring time.

In the working mode, the data of one work frequency can be divided into several segments, and there is a random phase difference between the two adjacent segments, which causes difficulties to extract Doppler information. The data coherence is destroyed by the random phase. On the other hand, the resolution cannot meet the system requirements if using traditional spectrum estimation algorithm for the subsegment, because the monitoring time of each subsegment is short. The resolution of modern spectral estimation technology has higher resolution than traditional method for small set of data [15]. Based on the modern spectral estimation algorithm, this paper proposes an S-MVDR algorithm to process the segment signals. This algorithm is also suitable for dealing with other segment signals, such as the signals of multiple piecewise chirp radar.

The paper is organized as follows. In Section 2, the echo model of sweep frequency radar system is established. In Section 3, the principles and calculation steps of the S-MVDR are presented. The simulation results of the S-MVDR are shown in Section 4. Finally, the conclusion is drawn in Section 5.

## 2. Radar Echo Signal Model.

**2.1. Coherent signal model.** HF radar usually adopts chirp signal or phased-coded signal. The following analysis takes the phased-coded signal as an example and denotes the transmitted signal by

$$S_t(t) = A \cdot \exp [j2\pi f_c t + j\varphi_p(t) + j\varphi_0] \quad (1)$$

where  $A$  is the amplitude of radar signal and we take it as 1 hereafter for convenience,  $f_c$  is transmitting frequency,  $\varphi_p(t)$  is phase modulation function, and  $\varphi_0$  is the initial phase

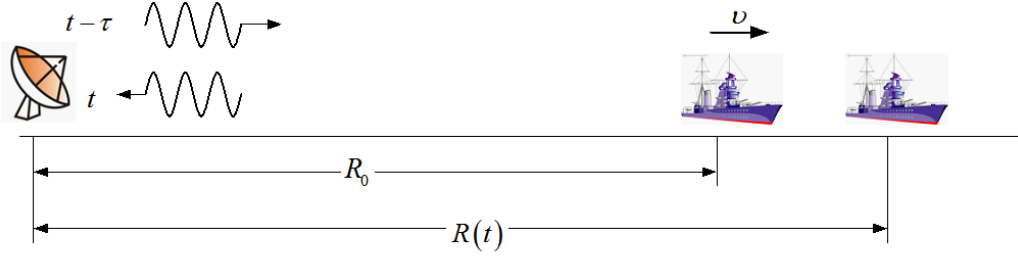


FIGURE 1. Illustration of radar echo

and it is an independent random variable subjected to the uniform distribution within  $[-\pi, \pi]$ .

The signal is received by the receiving antenna after being reflected from a target, and the receiving signal  $S_r(t)$  is expressed as

$$S_r(t) = S_T(t - \tau) = \exp [j2\pi f_c(t - \tau) + j\varphi_p(t - \tau) + j\varphi_0] \quad (2)$$

where  $\tau$  is the delay time between transmitted and received signal.

The distance between the radar and the target is a function of time if the target is in motion. Suppose that one single target deviates from the radar, as shown in Figure 1. On the moment, the distance  $R(t)$  is

$$R(t) = R_0 + vt \quad (3)$$

where  $v$  is the target velocity and  $R_0$  is the initial distance between the radar and target, which is also the distance when  $t = 0$ .

If we denote that the moment when signal is received is  $t$  and the moment when signal is transmitted is  $t - \tau$ , then the distance between the radar and target when the signal is reflected at  $t - \tau/2$  is

$$R(t - \tau/2) = R_0 + (t - \tau/2)v \quad (4)$$

The round-trip time  $\tau$  is

$$\tau = \frac{2R(t - \tau/2)}{c} = \frac{2[R_0 + (t - \tau/2)v]}{c} \quad (5)$$

where  $c$  is radio wave propagation speed in vacuum, which is  $3 \times 10^8$  m/s.

The solution of (5) is

$$\tau = \frac{2(R_0 + vt)}{c + v} \quad (6)$$

Taking Equation (6) into (2), the received signal can be rewritten as follows:

$$\begin{aligned} S_r(t) &= \exp \left[ j\varphi_p(t - \tau) + j2\pi f_c \left( t - \frac{2(R_0 + vt)}{c + v} \right) + j\varphi_0 \right] \\ &= \exp [j\varphi_p(t - \tau)] \cdot \exp \left[ j2\pi f_c \left( \frac{c - v}{c + v} t - \frac{2R_0}{c + v} \right) \right] \cdot \exp (j\varphi_0) \end{aligned} \quad (7)$$

It is known that the relationship between the target velocity and  $c$  is  $v \ll c$ ; therefore, we have

$$\frac{c - v}{c + v} = \frac{1 - v/c}{1 + v/c} = (1 - v/c) \left( 1 - \frac{v}{c} + \frac{v^2}{c^2} - \dots \right) = 1 - \frac{2v}{c} + \dots \approx 1 - \frac{2v}{c} \quad (8)$$

Substituting Equation (8) into (7), then  $S_r(t)$  is

$$\begin{aligned} S_r(t) &\approx \exp[j\varphi_p(t - \tau)] \cdot \exp\left[j2\pi f_c t - j2\pi f_c \frac{2v}{c}t - j4\pi f_c \frac{R_0}{c+v}\right] \cdot \exp(j\varphi_0) \\ &\triangleq \exp[j\varphi_p(t - \tau)] \cdot \exp[j2\pi f_c t - j2\pi f_D t + j\varphi_\tau] \cdot \exp(j\varphi_0) \end{aligned} \quad (9)$$

where  $f_D$  is the Doppler frequency which is defined as  $f_D \triangleq f_c \frac{2v}{c}$ ,  $\varphi_\tau$  is the phase factor caused by code delay and it is defined as  $\varphi_\tau = -4\pi f_c \frac{R_0}{c}$ .

Therefore, we obtain zero intermediate frequency baseband signal model:

$$S_I(t) = \exp[j\varphi_p(t - \tau)] \cdot \exp[j2\pi f_D t + j\varphi_\tau] \cdot \exp(j\varphi_0) \quad (10)$$

**2.2. Segment echo data model.** The radar system works in sweep frequency mode. After several sweep frequency cycles, the echo is segment signal for the same working frequency. Figure 2 shows the waveform schematic diagram of segment signal containing single frequency.

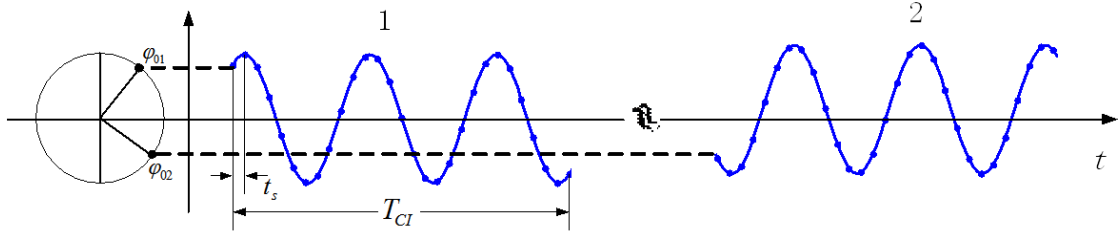


FIGURE 2. Scheme of segment signal waveform

In Figure 2,  $\varphi_{01}$  is the initial phase of subsegment 1, and  $\varphi_{02}$  is the initial phase of subsegment 2. It is clear that subsegment 1 and 2 are completely irrelevant. As a general rule, traditional algorithm cannot process the segment signal directly.

Since the multiple frequency components in the echo are additive, the segment signal model with multiple frequencies can be shown as follows:

$$S_D(t) = \sum_{l=1}^L \text{rect}\left[\frac{t - (l-1)T_{CPI}}{T_{CPI}}\right] \cdot \exp[j\varphi_p(t - \tau)] \cdot \exp[j(2\pi f_D t + \varphi_\tau)] \cdot \exp(j\varphi_{0l}) \quad (11)$$

where  $T_{CPI}$  is the monitoring time of one subsegment,  $L$  is the number of sweep frequency cycles,  $\{\varphi_{0l}\}$  is the initial phase of  $l$ th segment signal,  $\text{rect}$  is the rectangular window function.

The HFSWR segment signal can be rearranged into a two-dimensional matrix  $\mathbf{S}$ :

$$\mathbf{S} = \begin{bmatrix} \mathbf{S}_1 \\ \mathbf{S}_2 \\ \vdots \\ \mathbf{S}_M \end{bmatrix} = \begin{bmatrix} S_{1,1} & S_{1,2} & \cdots & S_{1,N} \\ S_{2,1} & S_{2,2} & \cdots & S_{2,N} \\ \vdots & \vdots & \ddots & \vdots \\ S_{M,1} & S_{M,2} & \cdots & S_{M,N} \end{bmatrix} \quad (12)$$

where  $M$  is the number of range cells,  $N$  is the number of sampling points, and  $S_{i,j}$  is the  $j$ th plural sample in the  $i$ th range cell.

According to the model, the echo data of one range cell is similar to sine signal sampling points. Therefore, the Doppler information can be extracted by Fourier transform in conventional method [16], and it is realized by FFT in engineering fields.

The resolution limit of the Fourier transform is the reciprocal of the CIT. In our system, the CIT of one subsegment is so short that the resolution cannot meet detecting requirements, if we estimate the spectrum of one subsegment with FFT. In addition, the accurate spectrum estimation results cannot be obtained by the subsegment data connected end to end because of the random phase differences. To improve resolution, we use modern signal spectrum estimation algorithm instead of FFT to extract the Doppler information.

### 3. S-MVDR Method.

**3.1. S-MVDR principle.** S-MVDR is put forward based on MVDR [17]. The time domain data  $\mathbf{y}$  processed in this paper is divided into  $L$  subsegments. For continuous sampling data, reference [18] puts forward twice coherent accumulate algorithm. However, in our system, there are data phase differences, so the second FFT is invalid. Here we propose an S-MVDR spectrum estimation method to solve this problem.

Assuming the segmentation data is

$$\mathbf{y} = [ \mathbf{y}_1 \quad \mathbf{y}_2 \quad \cdots \quad \mathbf{y}_L ] \tag{13}$$

where  $L$  is the number of segmentation or sweep frequency cycles in system, and  $y_i$  is echo data of  $i$ th subsegment.

Suppose that each subsegment has the same frequency compositions, but with different amplitude and phase. The  $i$ th subsegment signal  $y_i(t)$  is

$$y_i(t) = x_i(t) + e_i(t) \tag{14}$$

where  $x_i(t)$  is the noise free plural sine signal of  $i$ th subsegment, which can be written as follows:

$$\begin{aligned} x_i(t) &= \sum_{k=1}^n x_{ik}(t) \\ x_{ik}(t) &= \alpha_{ik} e^{j(\omega_k t + \varphi_{ik})} \end{aligned} \tag{15}$$

where  $x_{ik}(t)$  is the  $k$ th frequency component of  $x_i(t)$ ,  $\{\alpha_{ik}\}$  is the amplitudes,  $\{\varphi_{ik}\}$  and  $\{\omega_k\}$  are initial phase and angular frequency, and  $\{e_i(t)\}$  is additive noise of  $i$ th subsegment.

To develop the segment signal covariance matrix model, we define a vector  $\mathbf{a}$  and a matrix  $\mathbf{A}$ :

$$\mathbf{a}(\omega) \triangleq [ 1 \quad e^{-i\omega} \quad \cdots \quad e^{-i(m-1)\omega} ]^T \tag{16}$$

$$\mathbf{A} \triangleq [ \mathbf{a}(\omega_1) \quad \mathbf{a}(\omega_2) \quad \cdots \quad \mathbf{a}(\omega_n) ] \tag{17}$$

where  $m$  is an undetermined positive integer.

Shown in (17) is a Vandermonde matrix, when  $m \geq n$ ,  $\omega_k \neq \omega_p$  and  $k \neq p$ , the rank of  $\mathbf{A}$  satisfies  $\text{rank}(\mathbf{A}) = n$ .

From the sign given by (13)-(15), we have

$$\begin{aligned}
\tilde{\mathbf{y}}(t) &\triangleq \begin{bmatrix} y_1(t) & y_2(t) & \dots & y_L(t) \\ y_1(t-1) & y_2(t-1) & \dots & y_L(t-1) \\ \vdots & \vdots & & \vdots \\ y_1(t-m+1) & y_2(t-m+1) & \dots & y_L(t-m+1) \end{bmatrix} \\
&= \mathbf{A}\tilde{\mathbf{x}}(t) + \tilde{\mathbf{e}}(t) \\
\tilde{\mathbf{x}}(t) &\triangleq \begin{bmatrix} x_{11}(t) & x_{21}(t) & \dots & x_{L1}(t) \\ x_{12}(t) & x_{22}(t) & \dots & x_{L2}(t) \\ \vdots & \vdots & & \vdots \\ x_{1n}(t) & x_{2n}(t) & \dots & x_{Ln}(t) \end{bmatrix} \\
\tilde{\mathbf{e}}(t) &\triangleq \begin{bmatrix} e_1(t) & e_2(t) & \dots & e_L(t) \\ e_1(t-1) & e_2(t-1) & \dots & e_L(t-1) \\ \vdots & \vdots & & \vdots \\ e_1(t-m+1) & e_2(t-m+1) & \dots & e_L(t-m+1) \end{bmatrix}
\end{aligned} \tag{18}$$

Because  $x_{ik}$ 's initial phase  $\{\varphi_{ik}\}$  is subjected to the uniform distribution within  $[-\pi, \pi]$ , we have

$$\begin{aligned}
E \{ e^{j\varphi_{ip}} e^{j\varphi_{iq}} \} &= 1, \quad p = q \\
E \{ e^{j\varphi_{ip}} e^{j\varphi_{iq}} \} &= 0, \quad p \neq q
\end{aligned} \tag{19}$$

Then,

$$E \{ e^{j\varphi_{ip}} e^{j\varphi_{iq}} \} = \delta_{p,q} \tag{20}$$

Based on (20), the  $x_{ik}(t)$  shown in (15) can be written as follows:

$$E \{ x_{ip}(t) x_{iq}^*(t-k) \} = \alpha_p^2 e^{j\omega_{ip}k} \delta_{p,q} \tag{21}$$

The covariance matrix model of  $\tilde{\mathbf{y}}(t)$  can be deduced according to Equations (18) and (21):

$$\mathbf{R} \triangleq E \{ \tilde{\mathbf{y}}(t) \tilde{\mathbf{y}}^*(t) \} = \mathbf{A}\mathbf{P}\mathbf{A}^* + (\sigma_1^2 + \sigma_2^2 + \dots + \sigma_L^2)\mathbf{I} \tag{22}$$

where  $\mathbf{I}$  is  $n$  order unit matrix;  $\mathbf{P}$  is  $n$  order diagonal matrix, which is

$$\mathbf{P} = \begin{bmatrix} \alpha_{11}^2 + \alpha_{21}^2 + \dots + \alpha_{L1}^2 & & & \mathbf{0} \\ & \alpha_{12}^2 + \alpha_{22}^2 + \dots + \alpha_{L2}^2 & & \\ & & \ddots & \\ \mathbf{0} & & & \alpha_{1n}^2 + \alpha_{2n}^2 + \dots + \alpha_{Ln}^2 \end{bmatrix} \tag{23}$$

The  $i$ th element on  $\mathbf{P}$  diagonal  $\alpha_{1i}^2 + \alpha_{2i}^2 + \dots + \alpha_{Li}^2$  satisfies the quadratic sum of the  $i$ th frequency sine amplitude in all of the subsegments.  $\mathbf{R}$  contains all the information about frequencies  $\{\omega_{ik}\}$  of segment signals.

If we define  $\sigma_i^2$  as the noise variance of  $i$ th subsegment, and suppose the variance of each subsegment is equal, it turns out that

$$\sigma_1^2 = \sigma_2^2 = \dots = \sigma_L^2 = \sigma^2 \tag{24}$$

$$\mathbf{R} = E \{ \tilde{\mathbf{y}}(t) \tilde{\mathbf{y}}^*(t) \} = \mathbf{A}\mathbf{P}\mathbf{A}^* + L\sigma^2\mathbf{I} \tag{25}$$

Equation (25) is the segment signal covariance matrix model. According to Equations (23) and (25), it is clear that the covariance matrix model contains all the frequency information of each subsegment, and the amplitude of the same frequency is quadratic sum of each subsegment. In addition, the random phase of each subsegment does not affect the solution of  $\mathbf{R}$ .

The resolution of the algorithm is affected by the filter order  $m$ . Next we will process coherent signal  $y(0), y(1), \dots, y(N - 1)$  with the MVDR.

Here we define a matrix  $\mathbf{Y}(t)$  as

$$\mathbf{Y}(t) = \begin{bmatrix} y(t) \\ y(t-1) \\ \vdots \\ y(t-m) \end{bmatrix} [ y^*(t) \quad y^*(t-1) \quad \dots \quad y^*(t-m) ] \quad (26)$$

where  $m$  is a given positive integer.

In practical applications,  $\mathbf{R}$  will be replaced by a sample valuation, so the covariance matrix of  $y(0), y(1), \dots, y(N - 1)$  is

$$\hat{\mathbf{R}} = \frac{1}{N - m} \sum_{t=m+1}^N \mathbf{Y}(t) \quad (27)$$

As the rank of the product of two matrices is no more than the rank of either. And  $\mathbf{Y}$  is the product of two vectors, so we have

$$\text{rank}(\mathbf{Y}(t)) = 1, \quad t = m + 1, m + 2, \dots, N \quad (28)$$

Since the rank of matrixes sum is smaller than the sum of ranks of each matrix,  $\hat{\mathbf{R}}$  satisfies

$$\text{rank}(\hat{\mathbf{R}}) \leq \sum_{t=m+1}^N \text{rank}(\mathbf{Y}(t)) = N - m \quad (29)$$

Meanwhile, the necessary and sufficient condition of finding inverse matrix is that the original matrix is non-singular matrix. To make sure  $\hat{\mathbf{R}}^{-1}$  exist, we have

$$\text{rank}(\hat{\mathbf{R}}) = \dim(\hat{\mathbf{R}}) = m + 1 \quad (30)$$

According to Equations (29) and (30),  $m$  should satisfy

$$m < N/2 \quad (31)$$

The value of  $m$  determines the resolution limitation of the MVDR, so Equation (31) restricts the resolution limit.

Assuming that the segment signal contains  $L$  subsegments in the S-MVDR, and according to the covariance matrix model of segment signal, the covariance matrix  $\hat{\mathbf{R}}_s$  is

$$\hat{\mathbf{R}}_s = \frac{1}{N - m} \sum_{t=m+1}^N \sum_{i=1}^L \begin{bmatrix} y_i(t) \\ y_i(t-1) \\ \vdots \\ y_i(t-m) \end{bmatrix} [ y_i^*(t) \quad y_i^*(t-1) \quad \dots \quad y_i^*(t-m) ] \quad (32)$$

Let

$$\mathbf{Y}_i = \begin{bmatrix} y_i(t) \\ y_i(t-1) \\ \vdots \\ y_i(t-m) \end{bmatrix} [ y_i^*(t) \quad y_i^*(t-1) \quad \dots \quad y_i^*(t-m) ] \quad (33)$$

The rank of  $\hat{\mathbf{R}}_s$  should satisfy

$$\text{rank}(\hat{\mathbf{R}}_s) \leq \sum_{t=m+1}^N \sum_{i=1}^L \text{rank}(\mathbf{Y}_i(t)) = L(N - m) \quad (34)$$

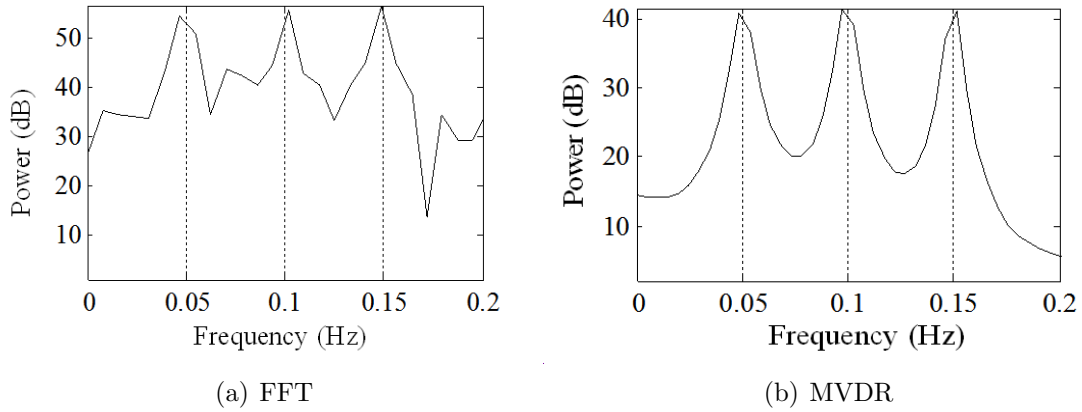


FIGURE 3. Power spectral of continuously monitored signal

According to (34), the restricted condition of  $m$  in the S-MVDR is

$$m < \frac{L}{L+1}N = \frac{1}{2}N + \frac{L-2}{L+1}N \quad (35)$$

It is clear that if the subsegment number  $L > 2$ , the filter order  $m$  in the S-MVDR is larger than that of the MVDR, and hence results in a higher resolution.

### 3.2. S-MVDR calculation steps.

Step 1. Construct segment time domain signal matrix according to (12).

Step 2. Construct segment signal covariance matrix estimation  $\hat{\mathbf{R}}_s$ .

Step 3. According to  $P(\omega) = \frac{m+1}{\mathbf{a}^H(\omega)\hat{\mathbf{R}}_s^{-1}\mathbf{a}(\omega)}$ , implement the spectrum estimation.

**4. Simulation Results.** The simulated signal  $S$  has three frequency components, which are  $f_1 = 0.05\text{Hz}$ ,  $f_2 = 0.1\text{Hz}$  and  $f_3 = 0.15\text{Hz}$ . The number of sampling points  $N$  is 640, the sampling time  $t_s$  is 0.2s, and within each subsegment the coherent integration time  $T_{CIT}$  is 128s. The spectrum estimation results are shown in Figure 3. The solid lines are spectrum density function curve, and the dotted lines are the actual signal frequency position. There are three peaks in Figures 3(a) and 3(b) resulted from FFT and MVDR respectively. It is clear that both the FFT and the MVDR can separate the three frequencies for long coherent signal.

If  $S$  is divided into five segments ( $L = 5$ ) as  $\{S_i\}$  ( $i = 1, 2, \dots, L$ ), and in each subsegment the number of sampling points  $N$  is 128. Then the spectrum of the first subsegment is re-estimated both by the FFT and MVDR, and the results are shown in Figure 4(a) and Figure 4(b) respectively. It can be seen that the FFT only has two peaks, because of the data shortage. In contrast, three frequencies can be distinguished in the MVDR but the signal to noise ratio (SNR) is low.

If we add a random initial phase to each segment  $\{S_i\}$  and form a segment data  $S'$  (in this situation, the data of all subsegments are coherent within the period and incoherent between each other), and constitute a new and long signal by the  $L$  segments connected directly, then we have the spectrum estimation results shown in Figure 5. From the FFT result shown in Figure 5(a), we can see that the three frequency peaks cannot be obtained accurately and there is a pseudo peak due to the phase differences. Though the MVDR can distinguish the three peaks, the deviation is huge.

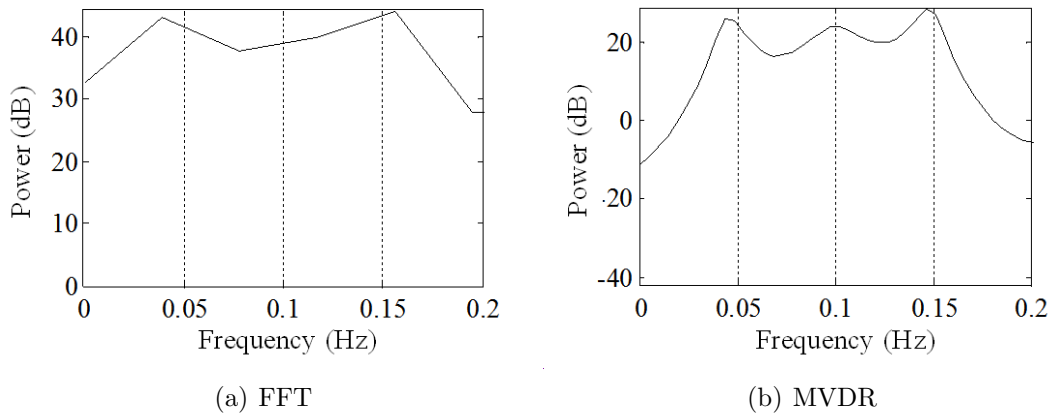


FIGURE 4. Power spectrum of one subsegment data

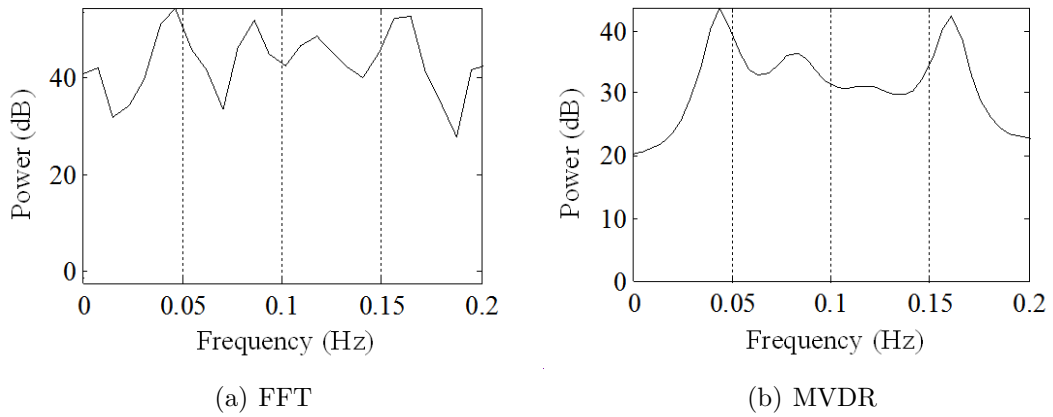


FIGURE 5. Power spectral of segment signal

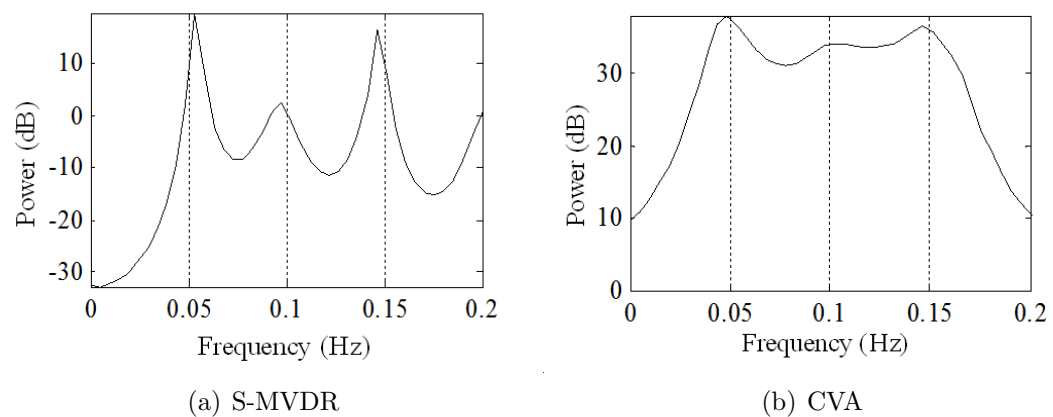


FIGURE 6. Power spectrum of segment data

Comparing the results of the S-MVDR with coherent accumulation within segment and video accumulation between segments of segment data with phase differences (here we call the method CVA for simplicity), results in Figures 6(a) and 6(b). It turns out that the S-MVDR can distinguish the exact frequency components with higher SNR.

TABLE 1. Comparison of various method

data	method	Peak position (Hz)			$\sigma_f^2$	SNR (dB)			SNR
$S$	FFT	0.047	0.1	0.148	$1.3e^{-5}$	15.78	17.28	17.72	16.93
	MVDR	0.049	0.098	0.151	$6e^{-6}$	21.19	19.64	21.50	20.776
$S_1$	FFT	unable to be distinguished							
	MVDR	0.044	0.102	0.147	$4.9e^{-5}$	13.25	11.10	16.01	13.45
$S'$	FFT	unable to be distinguished							
	MVDR	0.043	0.083	0.161	$4.59e^{-4}$	12.77	5.5	11.40	9.89
	CVA	0.048	0.102	0.147	$1.7e^{-5}$	10.69	6.74	9.19	8.87
	S-MVDR	0.053	0.098	0.147	$2.2e^{-5}$	24.75	9.48	22.18	18.80

**Note:** SNR is SNR mean of peaks.

Further, if we define  $\sigma_f^2$  is the peak frequency variance

$$\sigma_f^2 \triangleq \sum_{i=1}^K \left| \hat{f}_i - f_i \right|^2 \quad (36)$$

where  $K$  is the number of frequency components in the signal,  $\hat{f}_i$  is the  $i$ th frequency valuation,  $f_i$  is the theoretical frequency value, and  $\sigma_f^2$  represents the accuracy of frequency valuations.

Table 1 presents the results of various methods. It shows that both FFT and MVDR can distinguish the three frequency peaks for the long coherent data, but MVDR algorithm estimates the frequency more accurately and with higher SNR as well. For short data like  $S_1$ , FFT cannot distinguish the three peaks, and the SNR of MVDR is low. For the data  $S'$  with phase differences, if we connect the segments directly, FFT does not work, and the veracity and SNR of MVDR are limited, and  $\sigma_f^2$  is higher than  $S_1$ . When CVA is adopted, the veracity is better, but the SNR is still low. For the peculiar segment data model, S-MVDR proposed in this paper can improve the precision and SNR.

**5. Conclusions.** Interferences are dependent on radar frequency in the HFSWR, such as ionospheric clutter. They limit the radar detection performance and are difficult to suppress. The echo data of sweep frequency in the HFSWR can compensate for each other's detection blind zone caused by the interferences. However, the echo signal of sweep frequency in the HFSWR is distinct from the traditional system, and it makes the Doppler information hard to extract. This paper sets up an echo signal model of sweep frequency, and then analyzes its characteristics. In the model, the same frequency echo signals of sweep frequency system are composed by several subsegments. Within each subsegment the signal meets the coherent condition. However, there is random phase difference between each segment. According to the point target model, it is known that the essence of Doppler information extraction is the signal spectrum estimation. Traditional methods cannot extract the Doppler information because of the random phase in the sweep frequency signal model. For each subsegment, the resolution is too low because the coherent integration time is short. Therefore, to improve the resolution, this paper introduces a MVDR algorithm. Simulation results show that the MVDR algorithm has higher resolution than that of the Fourier transform, but it still cannot fully utilize all the segment data. Moreover, based on the MVDR, this paper proposes an S-MVDR algorithm. It is proved theoretically that the S-MVDR has higher resolution than the classical MVDR algorithm and without losing frequency information when applied with larger filter order. Simulation experiments demonstrate that the S-MVDR is more

powerful than any other algorithms in segment signal processing, and it solves the Doppler extraction problem in sweep frequency in the HFSWR.

**Acknowledgement.** The authors would like to express their appreciation and gratitude to the support of The National Natural Science Foundation of China (NSFC, Grant No. 61102158) and the Fundamental Research Funds for the Central Universities (HIT. NSRIF. Grant No. 2012022).

## REFERENCES

- [1] S. Maresca, M. Greco and F. Gini, The HF surface wave radar WERA. Part I: Statistical analysis of recorded data, *2010 IEEE Radar Conference*, Washington DC, USA, pp.826-831, 2010.
- [2] J. E. Khoury, R. Guinvarc'h and R. Gillard, Simulator of high frequency surface wave radar (HF-SWR) with offshore receiver, *2011 IEEE International Symposium on Antennas and Propagation (APSURSI)*, Spokane, WA, USA, pp.3241-3244, 2011.
- [3] W. Wang and L. R. Wyatt, Radio frequency interference cancellation for sea-state remote sensing by high-frequency radar, *IET radar, Sonar & Navigation*, vol.5, no.4, pp.405-415, 2011.
- [4] L. R. Wyatt, J. J. Green and A. Middleditch, Operational wave, current, and wind measurements with the pises HF radar, *IEEE J. Ocean Eng.*, vol.31, no.4, pp.819-834, 2006.
- [5] L. R. Wyatt, Limits to the inversion of HF radar backscatter for ocean wave measurement, *J. Atmos. Oceanic Technol.*, vol.17, no.12, pp.1651-1665, 2000.
- [6] W. Liu and S. Ding, Diagonal loading beamformers for pam communication systems, *International Journal of Innovative Computing, Information and Control*, vol.5, no.9, pp.2907-2916, 2009.
- [7] A. J. Abascal, S. Castanedo and V. Fernandez, Oil spill trajectory forecasting and backtracking using surface currents from high-frequency (HF) radar technology, *2011 IEEE – Spain OCEANS*, Santander, pp.1-8, 2011.
- [8] A. Dzvonkovskaya, K. W. Gurgel and H. Rohling, Low power high frequency surface wave radar application for ship detection and tracking, *2008 International Conference on Radar*, Adelaide, SA, pp.627-632, 2008.
- [9] G. Xin, S. Hongbo and Y. S. Tat, Interference cancellation for high-frequency surface wave radar, *IEEE Trans. on Geoscience and Remote Sensing*, vol.46, no.7, pp.1879-1891, 2008.
- [10] S. Shang, Z. Ning and L. Yang, Ionospheric clutter statistical properties in HFSWR, *Chinese Journal of Radio Science*, vol.26, no.3, pp.521-527, 2011.
- [11] Y. Li, N. Zhang and Q. Yang, Characteristic-knowledge-aided spectral detection of high frequency first-order sea echo, *Journal of Systems Engineering and Electronics*, vol.20, no.4, pp.718-725, 2009.
- [12] Y.-N. Chung, T.-C. Hsu, M.-L. Li, T.-S. Pan and C.-H. Hsu, A dynamic multiple-model estimator and neural algorithm for radar system, *International Journal of Innovative Computing, Information and Control*, vol.5, no.12(B), pp.4809-4817, 2009.
- [13] Z. Hao and W. Biyang, Analysis and suppression of ionosphere Es layer clutters in high-frequency surface wave radars, *Journal of Huazhong University of Science and Technology, Nature Science*, vol.39, no.4, pp.41-44, 2011.
- [14] W. Xianrong, K. Hengyu and W. Biyang, Adaptive ionospheric clutter suppression based on sub-rays in monostatic HF surface wave radar, *IEE Proc. of Radar, Sonar and Navigation*, vol.152, no.2, pp.89-96, 2005.
- [15] X. Zhang, X. Gao and D. Xu, Blind joint angle and frequency estimation with antenna array, *International Journal of Innovative Computing, Information and Control*, vol.5, no.6, pp.1681-1687, 2009.
- [16] L. Sun and A. Sano, System identification and error analysis in frequency domain, *International Journal of Innovative Computing, Information and Control*, vol.3, no.5, pp.1201-1218, 2007.
- [17] J. Capon, High resolution frequency-wavenumber spectrum analysis, *Proc. of the IEEE*, vol.57, no.8, pp.1408-1418, 1969.
- [18] Y. Wei, N. Xu and Y. Hou, Study on long-time integration algorithm for weak space-borne radar target, *Systems Engineering and Electronics*, vol.29, no.10, pp.1638-1642, 2007.